

Generating Fock-state superposition from coherent state by quantum measurement

Chen-yi Zhang¹ and Jun Jing^{1,*}

¹*School of Physics, Zhejiang University, Hangzhou 310027, Zhejiang, China*

(Dated: August 15, 2024)

High-level Fock states and their superpositions are essentially exotic testbeds for nonclassical physics and valuable resources for quantum technologies. We provide a simple protocol on quantum measurement to generate an arbitrary Fock state and selected superposed Fock states from a coherent state of a target resonator, without any carefully tailored external driving. This conditional protocol can be efficiently constructed by a sequence of joint free-evolution of the resonator and an ancillary qubit, that are coupled via a Jaynes-Cummings interaction, and projective measurements on the qubit. By properly choosing the duration of each evolution-measurement cycle and the initial state of the resonator, we can generate a desired Fock state $|n\rangle$ and a superposed Fock state $(|0\rangle + |n\rangle)/\sqrt{2}$, $n \sim 10$, with a fidelity over 99% in less than 30 measurements. Moreover, our protocol can be straightforwardly extended to the generation of a multi-excitation Bell state $(|00\rangle + |nn\rangle)/\sqrt{2}$ in a double-resonator system.

I. INTRODUCTION

A Fock state is of the most nonclassical state with a well-defined number of bosonic excitations such as photons, phonons, and magnons. It is found to play diverse and crucial roles in quantum information fields [1], including quantum communications [2], quantum metrology [3–6], and remote entanglement generation [7]. Fock states are prominent candidates in open quantum systems to explore the environment-induced decoherence by measuring their decay time [8, 9]. The superpositions of Fock states with particular components also exhibit appealing features in fault-tolerant quantum information processing [10]. For example, the superposed Fock states with binomial coefficients can be used in quantum error correction [11]. And a high-precision measurement over weak classical signals can be achieved by using superposed Fock states [12] due to the squeezing effect induced by quantum interference [13]. Generating desired Fock states and their superposition is therefore of significant interest to both the fundamental quantum physics and the applications in quantum technology.

Early proposals to generate Fock state employ the resonator and the ancillary atom in the Jaynes-Cummings (JC) model, which are under a full control in both initial states and coupling period. The atom serves as an intermediary between the resonator and the external driving pulse to pump quanta into the resonator by sequential half Rabi oscillations. The oscillation period depends on the current state of the resonator, by which the generation proposals demand elaborate external driving in the cavity QED setup [14, 15]. Based on such a step-wise method, Fock states and their superpositions were then experimentally generated in coplanar waveguide resonators for a microwave photon number $n \leq 6$ with a fidelity over 90% [16, 17] and in a bulk acoustic-wave resonator for up to $n = 7$ phonons with a fidelity over

26% [18]. In the transmon-cavity platform, Fock state with $n \leq 3$ can be generated by dispersively coupling the transmon-qubit to the photonic resonator and using a two-photon stimulated Raman adiabatic passage [19]. Two-level atomic systems are not necessary in the step-by-step idea. A proposal in Ref. [20] was presented to generate Fock state by the simultaneous adiabatic modulation over the driving frequency and intensity on a Kerr nonlinear cavity.

Beyond the methods based on multiple Rabi oscillations or equivalent transitions, Uria et al. considered in a cavity QED setup, a two-level atom resonantly coupled to the target cavity field initially prepared in a coherent state [21]. It had been numerically found that after a particular interaction period, the cavity field evolves into a displaced Fock state of a large photon number with a fidelity over 70%. Recently, the experimental demonstration of a dissipation engineering over a three-dimensional microwave cavity was reported in Ref. [22], which is based on a cascaded selective photon-addition operation assisted by an ancillary superconducting qubit and a readout resonator. The readout resonator was used to implement a quantum reservoir control for stabilizing a multiphoton Fock state of the cavity mode with a photon number up to $n = 3$ with a fidelity over 77%.

Quantum measurement is found to be a promising candidate for state control tasks, such as quantum state purification [23–25], ground state cooling of various quantum systems [26–28], and nuclear spin polarization [29]. Also, it can be implemented in generating Fock states by elaborate external tuning or by nondemolition measurements. For example, a Fock state of a cavity field can be conditionally created by the postselection over the atomic level after a specified period of evolution in a cavity QED setup, in which the atom-field interaction is highly tunable to control the transition rate in a chosen atom-field subspace on resonance [30]. An arbitrary superposed Fock state can be generated by the dispersive coupling between the cavity field and a qubit so that one could individually control the qubit transition rate associated with the corresponding qubit-field subspace by

* Email address: jingjun@zju.edu.cn

driving the qubit with external microwave signals containing multiple frequency components [31]. On performing quantum nondemolition measurement and feedback control over the field photon number to conditionally suppress the photon number spread in Fock space [32], a Fock state with a small photon number $n \leq 3$ was proposed in theory [33] and implemented in experiment [34]. Recently, quantum nondemolition measurement has been used in the preparation of a superposed Fock state in a circuit QED setup, which can be optimized by reinforcement learning [35].

With a JC Hamiltonian, we propose a protocol to conditionally generate a desired Fock states $|n\rangle$ and selected superposed Fock states, such as $(|0\rangle + |n\rangle)/\sqrt{2}$, of a target resonator that starts from the coherent state without extra cost in state preparation. The protocol is based on repeated performing projective measurements on the coupled qubit, which are separated with joint free-evolution of the composite system lasting a period of τ . For the resonator, the evolution-and-measurement cycles induce a positive operator valued measure (POVM) described by $V_{ji}(\tau) = \langle j|e^{-iH\tau}|i\rangle$, where $|i\rangle$ and $|j\rangle$ represent the initial state of the ancillary qubit and the measurement outcome, respectively and H denotes the full Hamiltonian of the composite system. Our protocol does not require any elaborate external parametric driving or tuning during the whole generation process. By appropriately choosing POVM and the period τ for each evolution-measurement cycle, the selected Fock components can be efficiently distinguished from the coherent state. By using qutrit instead of qubit and two nondegenerate resonators instead of a single one, our protocol can be extended to generate double-mode Fock states and multi-excitation Bell states $(|00\rangle + |nn\rangle)/\sqrt{2}$. In terms of the JC model and the projective measurement over the ancillary system, our work is inspired by previous proposals for generating nonclassical bosonic states, e.g., the Fock states and their classical mixtures in Refs. [36] and [37], respectively, and the squeezed state in Ref. [38]. Nevertheless, our protocol is applicable to generate superposed states and extendable to multiple modes.

The rest of this work is organized as follows. In Sec. II, we introduce the theoretical framework for POVM based on the JC model and repeated projective measurements on the ancillary qubit. We find the reduction factor on the population distribution of the resonator, which is crucial to the ensued state generation, is exclusively determined by the qubit-resonator coupling strength, their detuning, and the period of each evolution-and-measurement cycle. In Sec. III A and Sec. III B, we discuss the generation of various single-mode Fock states and their coherent superpositions, respectively. The protocol efficiency can be optimized by modulating the evolution periods. In Sec. IV, our protocol is extended to generate the double-mode Fock states or multi-excitation Bell state of two nondegenerate resonator modes with 2D population-reduction factors and strategies. We summarize the whole work in Sec. V.

II. THEORETICAL FRAMEWORK

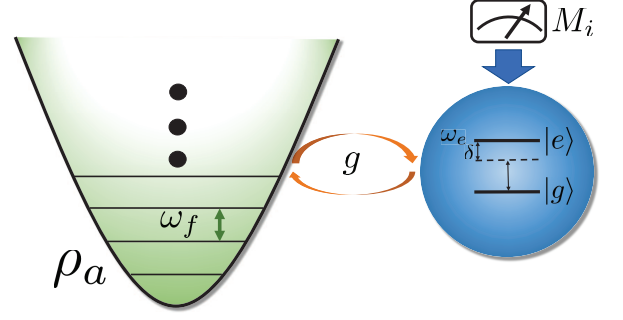


FIG. 1. Model diagram for our superposed Fock-state generation protocol. A two-level system (qubit) serves as the ancillary system. The target resonator is coupled to the qubit through exchange interaction with a strength g . δ is their detuning in frequency. The projective measurements $M_i = |i\rangle\langle i|$, $i = g, e$, are performed on the ancillary qubit.

Our protocol to generate the desired Fock states or their superposition of a single bosonic mode is based on a composite system consisting of a target resonator coupled to an ancillary qubit with a JC interaction, as shown in Fig. 1. The full Hamiltonian reads ($\hbar = 1$)

$$H = \omega_e |e\rangle\langle e| + \omega_f a^\dagger a + g (a^\dagger |g\rangle\langle e| + a |e\rangle\langle g|), \quad (1)$$

where ω_e and ω_f are the level splitting of the ancillary qubit and the transition frequency of the target resonator, respectively. a^\dagger (a) is the creation (annihilation) operator of the resonator. g denotes the qubit-resonator coupling strength. In the rotating frame with respect to $U_0 = \exp[i\omega_f(|e\rangle\langle e| + a^\dagger a)t]$. The Hamiltonian becomes

$$\begin{aligned} H' &= U_0 H U_0^\dagger - i U_0 \frac{\partial U_0^\dagger}{\partial t} \\ &= \delta |e\rangle\langle e| + g (a^\dagger |g\rangle\langle e| + a |e\rangle\langle g|), \end{aligned} \quad (2)$$

where $\delta \equiv \omega_e - \omega_f$ denotes the detuning between the qubit and the resonator mode.

Suppose that the ancillary qubit is prepared as one of its energy eigenstate $|i\rangle$, $i \in \{e, g\}$, and the resonator is initially at $\rho_a(0)$. After a period τ of joint free-evolution governed by $U(\tau) = \exp(-iH'\tau)$, we perform a projective measurement on the qubit. If the measurement outcome is $|j\rangle$, $j \in \{e, g\}$, the density matrix of the resonator is then found to be

$$\rho_a(\tau) = \frac{V_{ji}(\tau)\rho_a(0)V_{ji}^\dagger(\tau)}{\text{Tr}[V_{ji}(\tau)\rho_a(0)V_{ji}^\dagger(\tau)]} = \frac{V_{ji}(\tau)\rho_a(0)V_{ji}^\dagger(\tau)}{P_j(1)}, \quad (3)$$

where $V_{ji}(\tau) = \langle j|e^{-iH'\tau}|i\rangle$ denotes an effective (nonunitary) evolution operator acting on the resonator. And $P_j(1)$ represents the success probability of the ancillary qubit on the state $|j\rangle$ after an evolution-measurement cycle. In our protocol, the cycle is repeated if $|j\rangle = |i\rangle$.

Otherwise, the entire protocol is restarted from the very beginning.

The effective evolution operator $V_{ii}(\tau)$ then can be relabeled as $V_i(\tau)$ for simplicity, which is diagonal in the Fock-state basis $\{|k\rangle\}$, i.e.,

$$V_i(\tau) = \sum_{k=0}^{\infty} \lambda_k^{(i)}(\tau) |k\rangle \langle k|. \quad (4)$$

Here the coefficient $\lambda_k^{(i)}(\tau)$ is

$$\lambda_k^{(i)}(\tau) = e^{-i\delta\tau/2} \left[\cos \Omega_k^{(i)} \tau + i\delta \frac{\sin \Omega_k^{(i)} \tau}{2\Omega_k^{(i)}} \right], \quad (5)$$

where the k -photon Rabi frequency for $i = e, g$ are

$$\Omega_k^{(e)} = \sqrt{\delta^2/4 + (k+1)g^2}, \quad (6)$$

$$\Omega_k^{(g)} = \sqrt{\delta^2/4 + kg^2}. \quad (7)$$

respectively. Since $|\lambda_k^{(i)}(\tau)| \leq 1$, it works evidently as a reduction factor for the population on the Fock-state $|k\rangle$.

If the outcomes of each measurement are identical to the initial state of the qubit $|i\rangle$ and τ is invariant, the density matrix of the resonator under N rounds of evolution and measurement is found to be

$$\begin{aligned} \rho_a(N\tau) &= \frac{V_i^N(\tau) \rho_a(0) V_i^{\dagger N}(\tau)}{\text{Tr} \left\{ V_i^N(\tau) \rho_a(0) V_i^{\dagger N}(\tau) \right\}} \\ &= \mathcal{D}[\rho_a(N\tau)] + \mathcal{C}[\rho_a(N\tau)], \end{aligned} \quad (8)$$

$$\mathcal{D}[\rho_a(N\tau)] = \sum_{k=0}^{\infty} \frac{p_k |\lambda_k^{(i)}(\tau)|^{2N}}{P_i(N)} |k\rangle \langle k|, \quad (9)$$

$$\mathcal{C}[\rho_a(N\tau)] = \sum_{k \neq k'} \frac{C_{kk'} \left[\lambda_k^{(i)}(\tau) \lambda_{k'}^{(i)*}(\tau) \right]^N}{P_i(N)} |k\rangle \langle k'|, \quad (10)$$

where $\mathcal{D}[\rho_a]$ and $\mathcal{C}[\rho_a]$ denote the diagonal and off-diagonal parts of the density matrix, respectively. And $p_k \equiv \langle k | \rho_a(0) | k \rangle$ and $C_{kk'} \equiv \langle k | \rho_a(0) | k' \rangle$ are the populations and coherence of the initial density matrix of the resonator in the Fock-state basis $\{|k\rangle\}$. The success probability of finding the qubit at its initial state after N measurements is found to be

$$P_i(N) = \sum_{k=0}^{\infty} |\lambda_k^{(i)}(\tau)|^{2N} p_k. \quad (11)$$

According to Eqs. (9) and (10), one can find that the variation of both population p_k and coherence magnitude $C_{kk'}$ are determined by the coefficient $\lambda_k^{(i)}(\tau)$. It is noted that $\lambda_k^{(i)}(\tau)$ is independent on the resonator state, and yet depends on the evolution period τ , the resonator-qubit detuning δ , and the resonator-qubit coupling strength g . By optimizing the evolution period τ for each round of evolution and measurement, one can construct a filter preserving the desired elements in the density matrix of the resonator with $|\lambda_k^{(i)}(\tau)| = 1$ and in the same time eliminating the others with $|\lambda_k^{(i)}(\tau)| < 1$.

III. FOCK-STATE AND SUPERPOSED FOCK-STATE GENERATION IN SINGLE MODE

A. Fock-state generation

Our protocol to generate an arbitrary Fock state $|n\rangle$ can be performed with a sequence of projective measurements $M_e = |e\rangle\langle e|$ on the excited state of ancillary qubit. In the beginning of the each round of evolution and measurement, the qubit starts from $|e\rangle$. The initial density matrix of the full system reads

$$\rho(0) = |e\rangle\langle e| \otimes |\alpha\rangle\langle\alpha|, \quad |\alpha\rangle = \sum_{k=0}^{\infty} \alpha_k |k\rangle, \quad (12)$$

where $\alpha_k = e^{-|\alpha|^2/2} \alpha^k / \sqrt{k!}$. On substituting Eq. (5) into Eq. (9), the diagonal part of density matrix of the resonator after N rounds of equally-spaced evolution and measurement turns out to be

$$\mathcal{D}[\rho_a(N\tau)] = \sum_{k=0}^{\infty} \frac{|\alpha_k|^2 \cos^{2N} \Omega_k^{(e)} \tau |k\rangle \langle k|}{P_e(N)}. \quad (13)$$

The fidelity of the target Fock state $|n\rangle$ is found to be

$$\mathcal{F}(N) = \langle n | \rho_a(N\tau) | n \rangle = \frac{|\alpha_n|^2 \cos^{2N} \Omega_n^{(e)} \tau}{\sum_k |\alpha_k|^2 \cos^{2N} \Omega_k^{(e)} \tau}. \quad (14)$$

To generate the Fock state $|n\rangle$, the relevant population-reduction factor has to satisfy $|\lambda_n^{(e)}(l\tau_n^{(e)})|^2 = 1$. Due to Eq. (5) and the resonant assumption $\delta = 0$, the evolution period of a single round τ can be found as

$$\tau = l\tau_n^{(e)} = l \frac{\pi}{\Omega_n^{(e)}} = l \frac{\pi}{g\sqrt{n+1}}, \quad (15)$$

where $l \in \mathbb{N}^+$. If the irrelevant population-reduction factors $|\lambda_k^{(e)}(l\tau_n^{(e)})|^2$ for all the significantly occupied Fock states $|k\rangle$, $k \neq n$, are always less than unit, the resonator state will gradually approach the desired $|n\rangle$ as the round number N increases. The filter effect can be further amplified by the success probability $P_e(N) < 1$ in the denominator of Eq. (13). Therefore the density matrix of the resonator mode becomes

$$\rho_a(N\tau) \rightarrow \frac{|\alpha_n|^2}{P_e(N)} |n\rangle \langle n| = |n\rangle \langle n| \quad (16)$$

in the ideal large- N limit. Also it indicates that the success probability converges to the initial population of the target Fock-state:

$$P_e(N) \rightarrow |\alpha_n|^2 = e^{-|\alpha|^2} \frac{|\alpha|^{2n}}{n!}. \quad (17)$$

Besides the target state $|n\rangle$, also the populations on the Fock states $|n_j^{(l)}\rangle$ remain invariant when

$$n_j^{(l)} = \frac{j^2}{l^2} (n+1) - 1 \quad (18)$$

with $j \in \mathbb{N}^+$ due to Eqs. (5) and (15). The solution set with $l \neq 1$ covers that with $l = 1$. To perform strategies for Fock-state generation with varying τ or l in the sequence of measurements, we then focus on the intersection of the solution set with $l = 1$ and that with $l \neq 1$. Thus in the following, $n_j^{(l)}$ can be briefly labelled as n_j and it is readily to find that $n = n_1$. More generally, a sufficiently large number of evolution-measurement cycles with τ in Eq. (15) give rise to a stabilized subspace $\mathcal{V}_n^{(e)}$ spanned by $\{|n_j\rangle | j \in \mathbb{N}^+\}$, where both the populations and coherence elements are under protection in our protocol. To enhance the final success probability of the target Fock state, the initial coherent state $|\alpha\rangle$ of the resonator can be prepared with $|\alpha|^2 = n$ such that $|n\rangle$ is the maximally occupied Fock state and the populations on $|n_{j \geq 2}\rangle$ are negligible. For example, when $n = n_1 = 5$, the population on the next unwanted yet protected Fock state $n_2 = 23$ is about $p_{n_2} \sim 10^{-5}$.

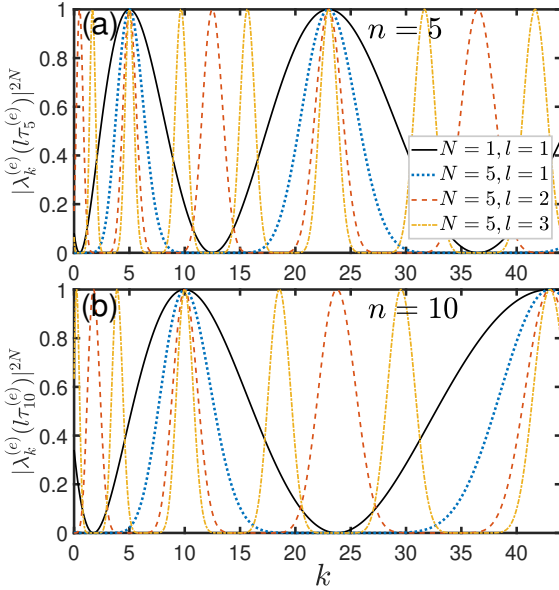


FIG. 2. Population-reduction factors as a function of the Fock index k after N evolution-measurement cycles with various evolution periods τ indicated by l . The target states are (a) $|n = 5\rangle$ and (b) $|n = 10\rangle$. The black solid lines indicate a single round with $\tau = \tau_n^{(e)}$ ($l = 1$). The blue dotted lines, the red dashed lines, and the yellow dash-dotted lines indicate $N = 5$ rounds with $\tau = \tau_n^{(e)}$, $\tau = 2\tau_n^{(e)}$ ($l = 2$), and $\tau = 3\tau_n^{(e)}$ ($l = 3$), respectively. $g = 0.05\omega_e$ and $\delta = 0$.

The efficiency for generating the target state is determined by the profile of the population-reduction factors $|\lambda_k^{(e)}(l\tau_n^{(e)})|^{2N}$ in the Fock space as shown in Figs. 2(a) and 2(b), where $n = 5$ and $n = 10$, respectively. These factors are evaluated under various periods τ of free-evolution (indicated by l) after N rounds of evolution and measurement. The black solid lines in Fig. 2 demonstrate the effect under a single projective measurement, confirming that the population-reduction factors of the irrelevant

Fock states $k \neq n_{j \geq 1}$ satisfy $|\lambda_k^{(e)}(\tau)|^2 < 1$. And the comparison between the blue dotted lines and the black solid lines suggests that the populations in the neighboring regions of $|n_j\rangle$ can be significantly suppressed by only 5 measurements.

Using multiples of τ (see the red dashed lines for $l = 2$ and the yellow dot-dashed line for $l = 3$), it is interesting to find that on one hand, they can intensify the population-reduction effect surrounding the target state $|n_1\rangle$ with a much concentrated population-protected region; yet on the other hand, more population-protected (although not strictly) Fock states arise, e.g., see the high profiles between $|n_1 = 5\rangle$ and $|n_2 = 23\rangle$ in Fig. 2(a). Those results suggest a compromise or hybrid strategy labelled with $\mathcal{S}_l^{(q)}$ that filters out the populations distributed on the states other than $|n_j\rangle$ by using $\tau = \tau_n^{(e)}$ in the first q rounds of evolution-and-measurement and then promotes the state-generation efficiency by using $\tau = l\tau_n^{(e)}$, $l > 1$, in the rest rounds. Often we take $l = 2$ or $l = 3$ since the advantage from an even larger l is not significant. Accordingly, the uniform strategy with an invariant period $\tau = \tau_n^{(e)}$ can be labelled with $\mathcal{S}_1^{(\infty)}$.

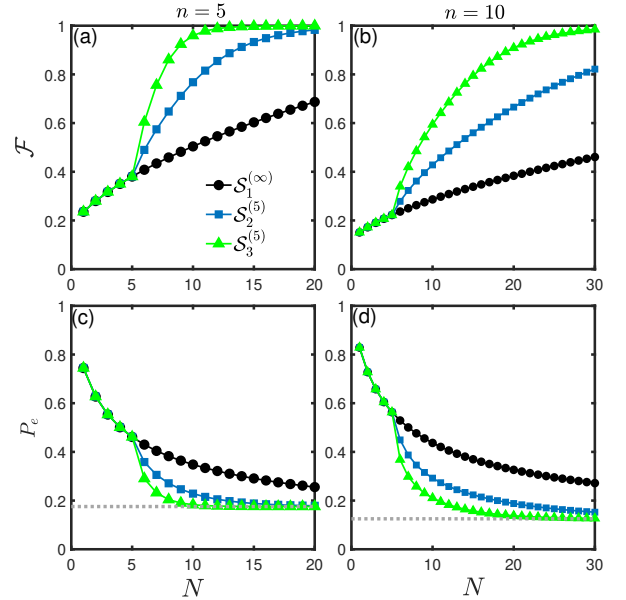


FIG. 3. Comparison of various strategies in Fock-state generation of (a) and (c): $|5\rangle$ and of (b) and (d): $|10\rangle$ as a function of the measurement number N . (a) and (b): Target-state fidelity. (c) and (d): Success probability, where the gray dotted lines indicate the initial population of $|n\rangle$. The system parameters are the same as Fig. 2.

In Fig. 3, we compare the efficiencies for generating the Fock state between the uniform strategy and the hybrid strategy $\mathcal{S}_l^{(5)}$ with $l = 2, 3$ in terms of the target-state fidelity $\mathcal{F}(N)$ and the success probability $P_e(N)$, whose definitions can be found in Eqs. (14) and (11), respectively. With the current hybrid strategy, the first $q = 5$

rounds of the evolution and measurement use $\tau = \tau_n^{(e)}$ and the rest rounds use $\tau = l\tau_n^{(e)}$. It is found that the hybrid strategy overwhelms the uniform one in the state fidelity under a limited number of measurements. And a larger l gives rise to an even better performance. In Fig. 3(a), the fidelity \mathcal{F} of the target Fock-state $|5\rangle$ can reach 99.6% within 15 measurements when $l = 3$. In contrast, \mathcal{F} reaches only 68.6% within 20 measurements by the uniform strategy. In Fig. 3(b), it is found that a higher Fock state $|10\rangle$ could be obtained by merely 30 measurements in the strategy $\mathcal{S}_3^{(5)}$ with a fidelity over 98.4%. Different strategy yields the same asymptotic value of the success probability, i.e., the population of $|n\rangle$ in the initial coherent state, which can be obtained by Eq. (17) with $|\alpha|^2 = n$. In both Figs. 3(c) and 3(d), a larger l gives rise to a faster convergence.

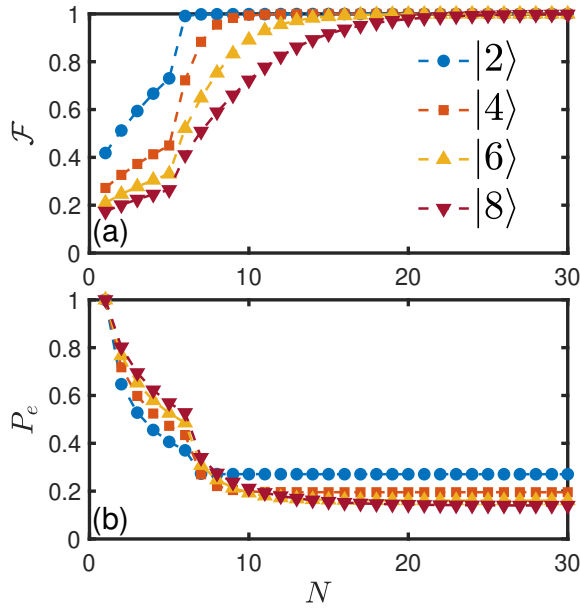


FIG. 4. Dependence of (a) Fidelity and (b) Success probability on the measurement number N under the strategy $\mathcal{S}_3^{(5)}$ for various target state. The system parameters are the same as Fig. 2.

In Fig. 4, we compare the performance for generating different Fock states under the hybrid strategy $\mathcal{S}_3^{(5)}$. And the initial coherent states are accordingly set with $|\alpha|^2 = n$. It is found in Fig. 4(a) that more rounds of evolution-measurement cycles are required to prepare a higher Fock states. That could be understood that a larger n indicates a broader population distribution in Fock space and a smaller overlap between the corresponding coherent state and the target state. For example, it requires only 6 rounds of evolution and measurement to enhance the fidelity of the target Fock state $|2\rangle$ to 99%, yet about 23 rounds to prepare $|8\rangle$ with almost the same fidelity. Figure 4(b) shows that the behavior of the success probability is insensitive to n . It declines rapidly

for the first few rounds and approaches the steady value after about $N = 10$ rounds.

B. Superposed Fock-state generation

Beyond the existing works for Fock state generation, our protocol can be used to prepare a superposed Fock state, such as

$$|\psi_{\pm}\rangle = c_0 |0\rangle \pm c_n |n\rangle, \quad (19)$$

with desired n , c_0 , and c_n . This target can be achieved by preparing the ancillary qubit in its ground state $|g\rangle$ and performing a sequence of projective measurements $M_g = |g\rangle\langle g|$ on the ancillary qubit. Due to Eqs. (4) and (5), the effective time-evolution operator for the resonator under the resonant condition $\delta = 0$ and an invariant τ is now written as,

$$V_g(\tau) = \sum_{k=0}^{\infty} \cos(\sqrt{k}g\tau) |k\rangle\langle k|. \quad (20)$$

In this case, the population on the vacuum state $|0\rangle$ of the resonator is always under protection due to the decoupling of the state $|g0\rangle$ from the other composite states in the time evolution. Using Eqs. (5) and (9), the diagonal part of the density matrix of the resonator after N rounds of equally-spaced evolution-and-measurement can be expressed by

$$\mathcal{D}[\rho_a(N\tau)] = \sum_{k=0}^{\infty} \frac{p_k \cos^{2N}(\sqrt{k}g\tau)}{P_g(N)} |k\rangle\langle k|, \quad (21)$$

$$P_g(N) = \sum_{k=0}^{\infty} p_k \cos^{2N}(\sqrt{k}g\tau), \quad (22)$$

where $P_g(N)$ denotes the success probability of finding the qubit still at its ground state after N measurements. Using Eq. (10), the off-diagonal part can be written as

$$\mathcal{C}[\rho_a(N\tau)] = \sum_{k \neq k'} \frac{C_{kk'} [\cos(\sqrt{k}g\tau) \cos(\sqrt{k'}g\tau)]^N}{P_g(N)} |k\rangle\langle k'|. \quad (23)$$

From Eqs. (19), (21), and (23), the fidelity \mathcal{F}_{\pm} about the target state $|\psi_{\pm}\rangle$ under N equally-spaced evolution-and-measurement rounds can be obtained as

$$\mathcal{F}_{\pm} = \left[|c_0|^2 p_0 + |c_n|^2 p_n \cos^{2N}(\sqrt{k}g\tau) \pm 2\text{Re}[C_{n0} c_0 c_n^*] \cos^N(\sqrt{k}g\tau) \right] / P_g(N). \quad (24)$$

Both populations on the ground state $|0\rangle$ and the Fock state $|n\rangle$ and their coherence should be under protection to generate the target superposed state $|\psi_{\pm}\rangle$ defined in

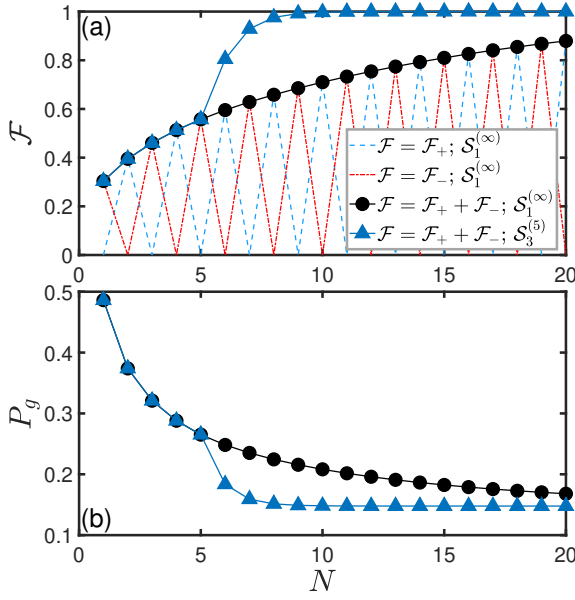


FIG. 5. (a) Fidelities \mathcal{F}_\pm for the target superposed state $(|0\rangle \pm |5\rangle)/\sqrt{2}$ or their combination $\mathcal{F}_+ + \mathcal{F}_-$ as functions of N under the uniform strategy $\mathcal{S}_1^{(\infty)}$ with $\tau = \tau_5^{(g)}$ and a hybrid strategy $\mathcal{S}_3^{(5)}$ that modifies the round period to be $\tau = 3\tau_5^{(g)}$ after 5 rounds of evolution and measurement. (b) Success probability of finding the qubit in its ground state after N measurements. The system parameters are the same as Fig. 2.

Eq. (19). To this end, the evolution periods for each round of evolution and measurement are selected as

$$\tau = l\tau_n^{(g)} = l\frac{\pi}{\Omega_n^{(g)}} = l\frac{\pi}{g\sqrt{n}}, \quad (25)$$

where $l \in \mathbb{N}^+$. With $l = 1$, a stabilized subspace under a full protection emerges under multiple measurements. It reads,

$$\mathcal{V}_n^{(g)} = \text{span}\{|0\rangle, |n\rangle, |2^2n\rangle, |3^2n\rangle, \dots\}. \quad (26)$$

The ratio of the probability amplitudes c_0/c_n is determined by α_0/α_n . Then inversely, one can find that the initial coherent state of the resonator is $|\alpha\rangle$ with $\alpha = (c_n\sqrt{n!}/c_0)^{1/n}$. Similar to the Fock-state generation described in Sec. III A, the initial populations on the Fock-state elements in the stabilized states $\{|j^2n\rangle | j \geq 2\}$ are negligible. Consequently, the diagonal and off-diagonal parts of the density matrix of the resonator in the large N limit read

$$\mathcal{D}[\rho_a(N\tau)] \rightarrow e^{-|\alpha|^2} \left(|0\rangle\langle 0| + \frac{|c_n|^2}{|c_0|^2} |n\rangle\langle n| \right) / P_g(N), \quad (27)$$

$$\mathcal{C}[\rho_a(N\tau)] \rightarrow e^{-|\alpha|^2} \left[\frac{c_n}{c_0} (-1)^N |n\rangle\langle 0| + \text{H.c.} \right] / P_g(N), \quad (28)$$

respectively, where the success probably approaches

$$P_g(N) \rightarrow p_0 + p_n = \exp \left[- \left(\frac{|c_n|}{|c_0|} \sqrt{n!} \right)^{\frac{2}{n}} \right] / |c_0|^2. \quad (29)$$

Eventually, the density matrix of the resonator results in

$$\rho_a(N\tau) = |c_0|^2 |0\rangle\langle 0| + |c_n|^2 |n\rangle\langle n| + [(-1)^N c_n c_0^* |n\rangle\langle 0| + \text{H.c.}] \quad (30)$$

by Eqs. (27), (28), and (29).

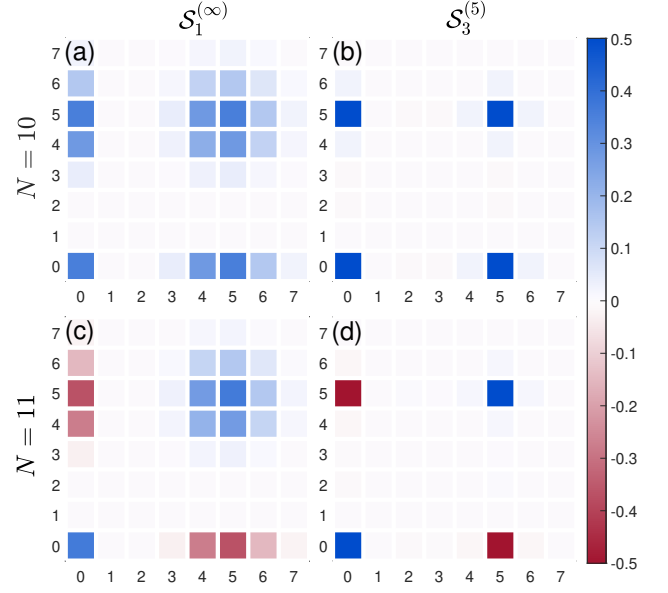


FIG. 6. Density matrix of the resonator after various rounds of evolution and measurement under (a) and (c) the uniform strategy with $\tau = \tau_5^{(g)}$ or (b) and (d) the hybrid strategy $\mathcal{S}_3^{(5)}$. In (a) and (b): $N = 10$; in (c) and (d): $N = 11$. The target state is $(|0\rangle \pm |5\rangle)/\sqrt{2}$ and other parameters are the same as in Fig. 2.

One can find that for $l = 1$ (generally for an odd l), the parity of N determines the output state is $|\psi_+\rangle$ or $|\psi_-\rangle$. In another word, after a sufficient large number of measurements, the resonator state will oscillate back and forth between $|\psi_+\rangle$ and $|\psi_-\rangle$ with an increasing fidelity. That alternate pattern can be observed by the blue dashed line and the red dot-dashed line in Fig. 5(a), which is consistent with Eq. (24). One can therefore employ a combination $\mathcal{F}_+ + \mathcal{F}_-$ to characterize the performance of our protocol. At the end of each round of evolution and measurement, $\mathcal{F}_+ + \mathcal{F}_- = \mathcal{F}_+(\mathcal{F}_-)$ for an even (odd) N . In Fig. 5(a), the fidelity $\mathcal{F}_+ + \mathcal{F}_-$ of the superposed state $(|0\rangle \pm |5\rangle)/\sqrt{2}$ is plotted with various strategy about the arrangement of τ . In the same spirit of the Fock-state generation in Sec. III A, the hybrid strategy displays a dramatic advantage over the uniform strategy. For example, the fidelity of the target state $|\psi_+\rangle$ reaches 99% with only $N = 10$ measurements under the strategy $\mathcal{S}_3^{(5)}$. In contrast, it is about 71% if τ remains as $\tau_5^{(g)}$ with

the same number of measurements. Figure 5(b) demonstrates the success probability of the qubit on its ground state $|g\rangle$ as a function of N . Again, the success probability using the hybrid strategy achieves the saturation value with a faster rate than the uniform strategy.

The difference between uniform and hybrid strategies in the superposed-state generation can be unambiguously described by the density matrix of the resonator. For either $|\psi_+\rangle$ in Figs. 6(a) and 6(b) or $|\psi_-\rangle$ in Figs. 6(c) and 6(d), which can be respectively prepared by $N = 10$ and $N = 11$ rounds of measurements, it is found that the hybrid strategy is superior to the uniform one.

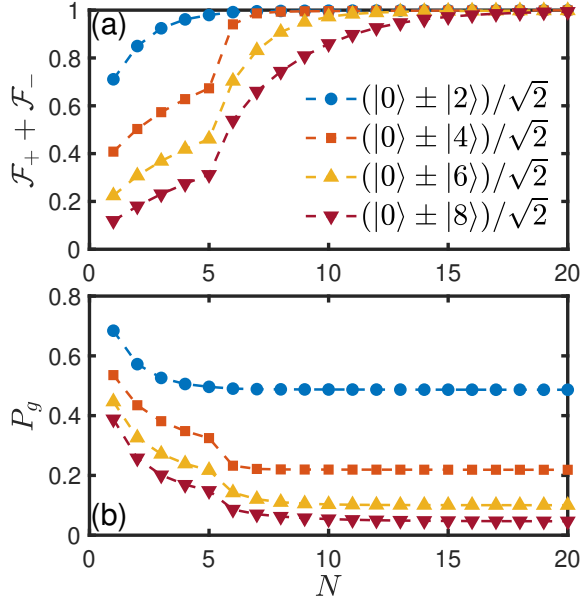


FIG. 7. Performance of our protocol in generating various superposed Fock states $(|0\rangle \pm |n\rangle)/\sqrt{2}$ with the hybrid strategy $\mathcal{S}_3^{(5)}$. (a): Fidelity of combination $\mathcal{F}_+ + \mathcal{F}_-$. (b) Success probability. The system parameters are the same as Fig. 2.

Fidelities for more superposed Fock states are plotted in Fig. 7(a). Similar to the result of the Fock-state generation, more rounds of evolution and measurement are required for a larger n . It costs $N = 6, 8, 14$, and 20 rounds of measurements to prepare the superposed states $(|0\rangle + |n\rangle)/\sqrt{2}$ of $n = 2, 4, 6$, and 8, respectively, with a fidelity over 99%. Note the population distribution of any coherent state (the initial state of the resonator) determines that it is hard to find in the same time sufficient occupations on both ground state $|0\rangle$ and Fock state $|n\rangle$ with a large n . In contrast, if one focuses on the Fock-state generation, it is then always possible to find a coherent state with a peak occupation on the desired $|n\rangle$. As one can expect from Eq. (29), the success probability of $(|0\rangle + |8\rangle)/\sqrt{2}$ in Fig. 7(b) is much lower than that of $|8\rangle$ in Fig. 4(b). In particular, the former is about 5% and the latter is about 14%. As expected, the success probability for the superposed state also decreases with increasing n .

IV. SUPERPOSED FOCK-STATE GENERATION IN DOUBLE MODES

Replacing the ancillary qubit with a V-type qutrit, our protocol for generating a single-resonator Fock state can be extended to a double-resonator system with frequencies $\omega_a \neq \omega_b$, as shown in Fig. 8. The ground state, the middle state, and the highest-level state of the ancillary system are denoted by $|g\rangle$, $|e\rangle$, and $|h\rangle$, respectively. And the resonator mode a (b) is only coupled to the transition $|g\rangle \leftrightarrow |h\rangle$ ($|g\rangle \leftrightarrow |e\rangle$) transition with a coupling strength g_a (g_b). $\delta_h = \omega_h - \omega_a$ and $\delta_e = \omega_e - \omega_b$ are the relevant detunings. In the rotating frame with respect to $U_0 = \exp\{i[\omega_a(a^\dagger a + |h\rangle\langle h|) + \omega_b(b^\dagger b + |e\rangle\langle e|)]t\}$, the full Hamiltonian reads,

$$H' = \delta_h |h\rangle\langle h| + \delta_e |e\rangle\langle e| + g_a(a^\dagger |g\rangle\langle h| + a |h\rangle\langle g|) + g_b(b^\dagger |g\rangle\langle e| + b |e\rangle\langle g|), \quad (31)$$

where a^\dagger (b^\dagger) and a (b) are the creation and annihilation operators for the resonator mode a (b), respectively.

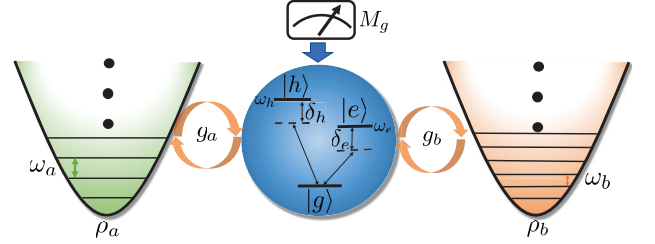


FIG. 8. Extended model diagram for our superposed Fock-state generation protocol, in which a V-type three-level system (qutrit) is coupled to two nondegenerate resonator modes. The projective measurements $M_g = |g\rangle\langle g|$ performing on the ancillary qutrit can steer the double modes towards a multi-excitation Bell state.

Our target is to generate a double-mode superposed Fock-state $|\psi_\pm\rangle = c_{00}|0\rangle_a|0\rangle_b \pm c_{mn}|m\rangle_a|n\rangle_b$ (briefly labelled as $c_{00}|00\rangle \pm c_{mn}|mn\rangle$ in the following), which is essentially a general Bell state of multiple excitations. The qutrit is initially at the ground state $|g\rangle$. And the two resonators a and b are prepared in coherent states $|\alpha\rangle$ and $|\beta\rangle$, respectively. To obtain the target state with desired amplitudes c_{00} and c_{mn} , it is straightforward to find that $\alpha = (c_{mn}m!/c_{00})^{1/2m}$ and $\beta = (c_{mn}n!/c_{00})^{1/2n}$, in a similar way to generating a single-mode superposed state.

After N rounds of evolution and measurement with a constant period τ and the measurement operator $M_g = |g\rangle\langle g|$, the state of resonators reads

$$\rho_{ab}(N\tau) = \frac{\Pi_g^N(\tau)|\alpha\rangle\langle\alpha| \otimes |\beta\rangle\langle\beta| \Pi_g^N(\tau)}{P_g(N)}, \quad (32)$$

where $\Pi_g(\tau) = \langle g|e^{-iH'\tau}|g\rangle$ denotes the effective time-evolution operator for the target resonators. $\Pi_g(\tau)$ is diagonal in the double-mode Fock basis $\{|kk'\rangle \equiv |k\rangle_a|k'\rangle_b\}$.

And $P_g(N)$ is the success probability that the qutrit remains at its ground state after N measurements. To find a compact expression for the measurement operator, we set $\delta_g = \delta_e = \delta$. Then we have

$$\Pi_g(\tau) = \sum_{k,k'} \lambda_{kk'}(\tau) |kk'\rangle \langle kk'|, \quad (33)$$

where the coefficients are

$$\lambda_{kk'}(\tau) = e^{-i\frac{\delta\tau}{2}} \left(\cos \Omega_{kk'}\tau + i \frac{\delta}{2\Omega_{kk'}} \sin \Omega_{kk'}\tau \right), \quad (34)$$

$$\Omega_{kk'} = \sqrt{\frac{\delta^2}{4} + g_a^2 k + g_b^2 k'}. \quad (35)$$

Using Eqs. (32) and (33), the diagonal part of the density matrix of the two resonator modes a and b in the basis $\{|kk'\rangle\}$ after N rounds of equally spaced evolution and measurement is found to be

$$\mathcal{D}[\rho_{ab}(N\tau)] = \sum_{k,k'} \frac{|\lambda_{kk'}(\tau)|^{2N} p_{kk'}}{P_g(N)} |kk'\rangle \langle kk'|, \quad (36)$$

where $p_{kk'} \equiv \langle kk' | \rho_a(0) \otimes \rho_b(0) | kk' \rangle$ is their initial population and the success probability turns out to be

$$P_g(N) = \sum_{k,k'} |\lambda_{kk'}(\tau)|^{2N} p_{kk'}. \quad (37)$$

The population-reduction factor on the double-mode Fock-states $|kk'\rangle$ is determined by the modulus square of the coefficients $|\lambda_{kk'}(\tau)|^2$. The matrix elements of off-diagonal part reads

$$\langle kk' | \mathcal{C}[\rho_a(N\tau)] | mm' \rangle = \frac{C_{kk',mm'} [\lambda_{kk'}(\tau) \lambda_{mm'}^*(\tau)]^N}{P_g(N)}, \quad (38)$$

where $C_{kk',mm'} \equiv \langle kk' | \rho_a(0) \otimes \rho_b(0) | mm' \rangle$ represents the coherence of the initial state.

Under the resonant condition $\delta = 0$, it turns out that $\lambda_{00}(\tau) = 1$, irrespective to the evolution period τ . In this case, $|g00\rangle$ is decoupled from all the other states of the composite system. From Eqs. (36) and (38), the fidelity of the target states $|\psi_{\pm}\rangle$ is found to be

$$\mathcal{F}_{\pm} = \left[|c_{00}|^2 p_{00} + |c_{mn}|^2 p_{mn} \cos^2 N(\Omega_{mn}\tau) \pm 2 \text{Re}(c_{mn}^* c_{00} C_{mn,00}) \cos^N(\Omega_{mn}\tau) \right] / P_g(N). \quad (39)$$

To generate $|\psi_{\pm}\rangle = c_{00}|00\rangle \pm c_{mn}|mn\rangle$, or equivalently to preserve both the population on $|mn\rangle$ and the coherence between $|00\rangle$ and $|mn\rangle$, the evolution period τ for each round of evolution and measurement can be chosen as $\tau = l\tau_{mn} = l\pi/\Omega_{mn}$ with $l \in \mathbb{N}^+$ to guarantee the condition $|\lambda_{mn}(\tau)| = 1$. When l is odd, the parity of N will determine whether or not a π phase presents in the coherence $\langle 00 | \mathcal{C}[\rho_a(N\tau)] | mn \rangle$, i.e., the outcome state is $|\psi_+\rangle$ or $|\psi_-\rangle$. And similar to the preceding situations,

the asymptotic success probability is equivalent to the overlap between the target states and the initial state of the resonator system. It is found to be

$$P_g(N) \rightarrow |\alpha_0 \beta_0|^2 + |\alpha_m \beta_n|^2$$

$$= \exp \left[- \left(\frac{|c_{mn}|}{|c_{00}|} n! \right)^{1/n} - \left(\frac{|c_{mn}|}{|c_{00}|} m! \right)^{1/m} \right] / |c_{00}|^2. \quad (40)$$

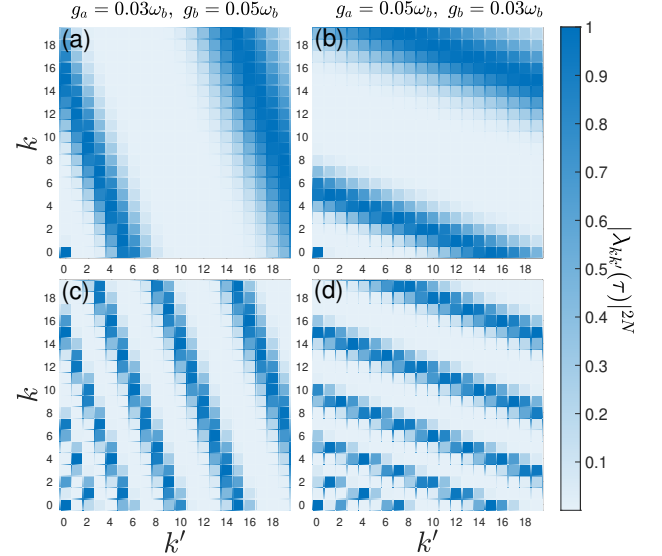


FIG. 9. 2D population-reduction factors $|\lambda_{kk'}(\tau)|^{2N}$ with $N = 5$ in the double-mode Fock-state basis $\{|kk'\rangle\}$ under various coupling strengths and measurement intervals. In (a) and (c), $g_a = 0.03\omega_b$ and $g_b = 0.05\omega_b$; and in (b) and (d): $g_a = 0.05\omega_b$ and $g_b = 0.03\omega_b$. In (a) and (b), $\tau = \tau_{44}$; and in (c) and (d): $\tau = 3\tau_{44}$.

Different from the single-mode Fock-state generation in Sec. III A, we have an extra degree of freedom in modulating the efficiency for generation of a double-mode state, since the double-mode population reduction factor $|\lambda_{kk'}(\tau)|^{2N}$ actually has a two-dimensional profile, as shown in Fig. 9. The target state is supposed to be, e.g., $|\psi_{\pm}\rangle = c_{00}|00\rangle \pm c_{44}|44\rangle$. Although many states other than the desired Fock states $|00\rangle$ and $|44\rangle$ also present with a unit or close-to-unit population-reduction factor. One can find in Fig. 9 that these unwanted states living in the dark-blue areas are distributed along the lines with a slope $-g_b/g_a$ passing through the point $(4j^2, 4j^2)$, $j \in \mathbb{N}^+$. Note in Figs. 9(a) and 9(b), we have $g_a/g_b = 3/5$ and $g_a/g_b = 5/3$, respectively. The two profiles are dramatically different from each other while their crossing points are the desired Fock states $|00\rangle$ and $|44\rangle$. A solution to reduce the populations on the unwanted states is then to alter the ratio of the two coupling strengths in the whole sequence of evolution-and-measurement rounds.

Similar to the single-mode case (see Fig. 2), a longer evolution period τ , i.e., a larger l , results in a more concentrated population-protected regions in Fock space, in-

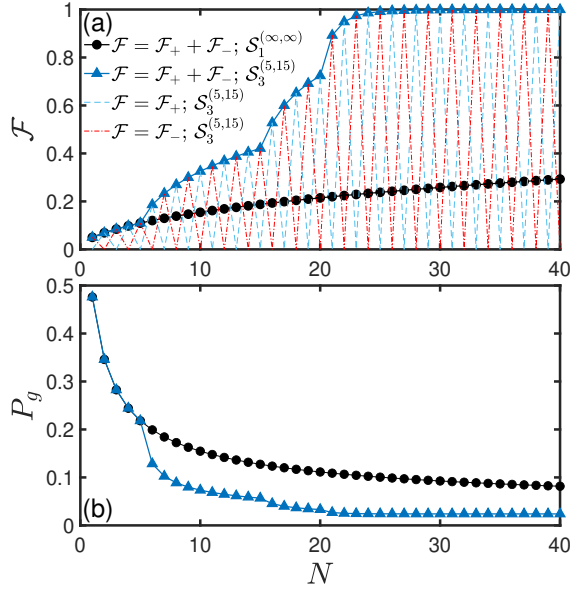


FIG. 10. (a) Fidelities of the target state $(|00\rangle \pm |44\rangle)/\sqrt{2}$ after N rounds of evolution and measurement under the uniform strategy with fixed $\tau = \tau_{44}$, $g_a = 0.05\omega_b$, and $g_b = 0.03\omega_b$ or the hybrid strategy $S_3^{(5, 15)}$, in which the coupling strengths $g_a = 0.05\omega_b$ and $g_b = 0.03\omega_b$ are modified to be $g_a = 0.03\omega_b$ and $g_b = 0.05\omega_b$ after $L = 15$ rounds of measurements. (b) Success probability of finding the qutrit in its ground state after N rounds.

dicating a higher generation efficiency. However, it also gives rise to more number of population protected regions. These two features can be identified in Figs. 9(c) and 9(d) by comparing to Figs. 9(a) and 9(b), respectively. Thus in regard of the 2D profile of population-reduction ratio, the hybrid strategy for the single-mode case is updated to have various ratio of the coupling strengths g_a/g_b and various period τ . It can be relabelled as $S_l^{(q, L)}$, $L > q$. The coupling ratio g_a/g_b is modified from 5/3 to 3/5 after L rounds of measurements; and the round period is $\tau = \tau_{mn}$ for $1 \leq N \leq q$ and $L + 1 \leq N \leq L + q$ and becomes $\tau = l\tau_{mn}$ for the rest rounds. The uniform strategy with invariant $\tau = \tau_{mn}$ and $g_a/g_b = 5/3$ can be labelled as $S_1^{(\infty, \infty)}$.

In Fig. 10(a), we present the fidelity of the target state $(|00\rangle \pm |44\rangle)/\sqrt{2}$ as a function of the measurement number N under either the uniform strategy or the hybrid strategy $S_3^{(5, 15)}$. \mathcal{F}_+ and \mathcal{F}_- manifest the same alternate pattern for N of different parity as in Fig. 5(a). With respect to the combination $\mathcal{F}_+ + \mathcal{F}_-$, the hybrid strategy $S_3^{(5, 15)}$ demonstrates a significant advantage over the uniform strategy. With 30 rounds of measurements, the former can prepare a general Bell state with a fidelity over 99%, while the latter attains only 25% in fidelity. Figure 10(b) indicates the cost of the target-state preparation, in which the success probability is stabilized around about 3% after about 25 rounds of evolution and measurement.

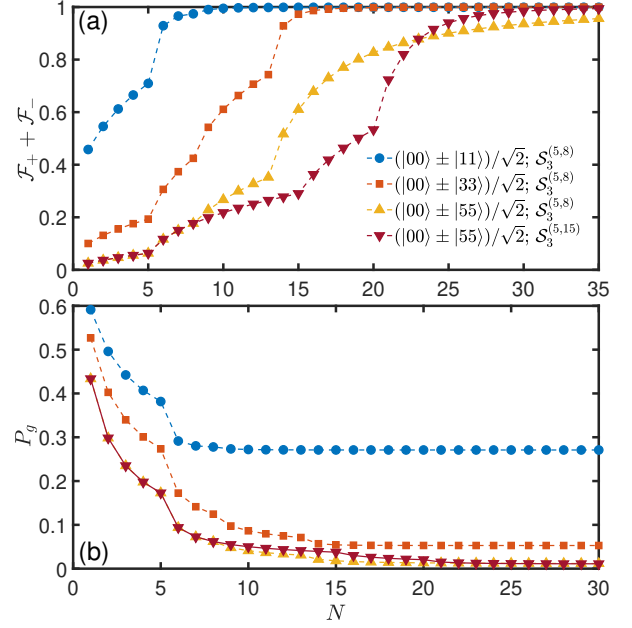


FIG. 11. Performance of our protocol in generating various multi-excitation Bell states $(|00\rangle + |nn\rangle)/\sqrt{2}$ under various hybrid strategy. (a): Combination fidelity $\mathcal{F}_+ + \mathcal{F}_-$. (b) Success probability. The system parameters are the same as Fig. 10.

In Fig. 11, we show the performance of our protocol in generating Bell states $(|00\rangle + |nn\rangle)/\sqrt{2}$ with $n = 1, 3$, and 5 under various hybrid strategy. Under the same strategy $S_3^{(5, 8)}$, the fidelities of the target states with $n = 1$ and $n = 3$ reach 99% after $N = 9$ and $N = 14$ rounds of measurements. And their success probabilities approach 28% and 6%, respectively. It is evident that it is harder to prepare a general Bell state with a larger n . The comparison between different strategies on the same target state $(|00\rangle + |55\rangle)/\sqrt{2}$ indicates that it is nontrivial to select a proper strategy in state generation. During the first L rounds with a constant ratio $g_a/g_b = 5/3$, the unwanted yet protected populations should be sufficiently suppressed. Otherwise, the performance as a whole will become less optimized. That could explain why the final fidelity under $S_3^{(5, 8)}$ is lower than that under $S_3^{(5, 15)}$. In the latter case, one can prepare $(|00\rangle + |55\rangle)/\sqrt{2}$ by $N = 33$ rounds of measurements with a fidelity over 99%.

V. CONCLUSION

In summary, we design a protocol based on a sequence of projective measurements on the ancillary atomic system to generate desired Fock states and superposed Fock states from a coherent state of a resonator. The measurements are separated by dozens of joint free evolutions of the resonator and the ancillary system that are coupled with a simple JC interaction. Through the analysis

over the population reduction factors induced by the effective time-evolution operator for the target resonator, we can find optimal strategies with varying duration of the evolution-and-measurement cycles. Our protocol can therefore utilize less than 30 measurements to create a Fock state $|n\rangle$ or a superposed Fock state $(|0\rangle + |n\rangle)/\sqrt{2}$ of $n \sim 10$ with a close-to-unit fidelity. The success probability of our conditional protocol is exclusively determined by the overlap between the initial state and the target state of the resonator. Moreover, the protocol can be generalized to prepare a multi-excitation Bell state in a double-resonator system assisted by a qutrit. Our work

thus proves quantum measurement to be a powerful tool to manipulate composite systems and presents a path to the generation of high-level Fock states and entangled states.

ACKNOWLEDGMENTS

We acknowledge grant support from the National Natural Science Foundation of China (Grant No. 11974311).

-
- [1] Y. Yamamoto and H. A. Haus, *Preparation, measurement and information capacity of optical quantum states*, *Rev. Mod. Phys.* **58**, 1001 (1986).
 - [2] C. M. Caves and P. D. Drummond, *Quantum limits on bosonic communication rates*, *Rev. Mod. Phys.* **66**, 481 (1994).
 - [3] M. J. Holland and K. Burnett, *Interferometric detection of optical phase shifts at the heisenberg limit*, *Phys. Rev. Lett.* **71**, 1355 (1993).
 - [4] T. Nagata, R. Okamoto, J. L. O'Brien, K. Sasaki, and S. Takeuchi, *Beating the standard quantum limit with four-entangled photons*, *Science* **316**, 726 (2007).
 - [5] V. Giovannetti, S. Lloyd, and L. Maccone, *Advances in quantum metrology*, *Nat. Photonics* **5**, 222 (2011).
 - [6] S. Slussarenko, M. M. Weston, H. M. Chrzanowski, L. K. Shalm, V. B. Verma, S. W. Nam, and G. J. Pryde, *Unconditional violation of the shot-noise limit in photonic quantum metrology*, *Nat. Photonics* **11**, 700 (2017).
 - [7] A. Narla, S. Shankar, M. Hatridge, Z. Leghtas, K. M. Sliwa, E. Zayls-Geller, S. O. Mundhada, W. Pfaff, L. Frunzio, R. J. Schoelkopf, and M. H. Devoret, *Robust concurrent remote entanglement between two superconducting qubits*, *Phys. Rev. X* **6**, 031036 (2016).
 - [8] H. Wang, M. Hofheinz, M. Ansmann, R. C. Bialczak, E. Lucero, M. Neeley, A. D. O'Connell, D. Sank, J. Wenner, A. N. Cleland, and J. M. Martinis, *Measurement of the decay of fock states in a superconducting quantum circuit*, *Phys. Rev. Lett.* **101**, 240401 (2008).
 - [9] M. Brune, J. Bernu, C. Guerlin, S. Deléglise, C. Sayrin, S. Gleyzes, S. Kuhr, I. Dotsenko, J. M. Raimond, and S. Haroche, *Process tomography of field damping and measurement of fock state lifetimes by quantum nondemolition photon counting in a cavity*, *Phys. Rev. Lett.* **101**, 240402 (2008).
 - [10] A. Joshi, K. Noh, and Y. Y. Gao, *Quantum information processing with bosonic qubits in circuit qed*, *Quantum Sci. Technol.* **6**, 031001 (2021).
 - [11] M. H. Michael, M. Silveri, R. T. Brierley, V. V. Albert, J. Salmilehto, L. Jiang, and S. M. Girvin, *New class of quantum error-correcting codes for a bosonic mode*, *Phys. Rev. X* **6**, 031006 (2016).
 - [12] C. M. Caves, K. S. Thorne, R. W. P. Drever, V. D. Sandberg, and M. Zimmermann, *On the measurement of a weak classical force coupled to a quantum-mechanical oscillator. i. issues of principle*, *Rev. Mod. Phys.* **52**, 341 (1980).
 - [13] K. Wódkiewicz, P. L. Knight, S. J. Buckle, and S. M. Barnett, *Squeezing and superposition states*, *Phys. Rev. A* **35**, 2567 (1987).
 - [14] K. Vogel, V. M. Akulin, and W. P. Schleich, *Quantum state engineering of the radiation field*, *Phys. Rev. Lett.* **71**, 1816 (1993).
 - [15] C. K. Law and J. H. Eberly, *Arbitrary control of a quantum electromagnetic field*, *Phys. Rev. Lett.* **76**, 1055 (1996).
 - [16] M. Hofheinz, E. M. Weig, M. Ansmann, R. C. Bialczak, E. Lucero, M. Neeley, A. D. O'Connell, H. Wang, J. M. Martinis, and A. N. Cleland, *Generation of fock states in a superconducting quantum circuit*, *Nature (London)* **454**, 310 (2008).
 - [17] M. Hofheinz, H. Wang, M. Ansmann, R. C. Bialczak, E. Lucero, M. Neeley, A. D. O'Connell, D. Sank, J. Wenner, M. J. M., and C. A. N., *Synthesizing arbitrary quantum states in a superconducting resonator*, *Nature (London)* **459**, 546 (2009).
 - [18] Y. Chu, P. Kharel, T. Yoon, L. Frunzio, P. T. Rakich, and R. J. Schoelkopf, *Creation and control of multiphonon fock states in a bulk acoustic-wave resonator*, *Nature (London)* **563**, 660 (2018).
 - [19] S. P. Premaratne, F. C. Wellstood, and B. S. Palmer, *Microwave photon fock state generation by stimulated raman adiabatic passage*, *Nat. Commun.* **8**, 14148 (2017).
 - [20] R. Yanagimoto, E. Ng, T. Onodera, and H. Mabuchi, *Adiabatic fock-state-generation scheme using kerr non-linearity*, *Phys. Rev. A* **100**, 033822 (2019).
 - [21] M. Uria, P. Solano, and C. Hermann-Avigliano, *Deterministic generation of large fock states*, *Phys. Rev. Lett.* **125**, 093603 (2020).
 - [22] S. Li, Z. Ni, L. Zhang, Y. Cai, J. Mai, S. Wen, P. Zheng, X. Deng, S. Liu, Y. Xu, and D. Yu, *Autonomous stabilization of fock states in an oscillator against multiphoton losses*, *Phys. Rev. Lett.* **132**, 203602 (2024).
 - [23] H. Nakazato, T. Takazawa, and K. Yuasa, *Purification through zeno-like measurements*, *Phys. Rev. Lett.* **90**, 060401 (2003).
 - [24] J. Combes, H. M. Wiseman, K. Jacobs, and A. J. O'Connor, *Rapid purification of quantum systems by measuring in a feedback-controlled unbiased basis*, *Phys. Rev. A* **82**, 022307 (2010).
 - [25] H. M. Wiseman and J. F. Ralph, *Reconsidering rapid qubit purification by feedback*, *New J. Phys.* **8**, 90 (2006).

- [26] Y. Li, L.-A. Wu, Y.-D. Wang, and L.-P. Yang, *Nondestructive ultrafast ground-state cooling of a mechanical resonator*, *Phys. Rev. B* **84**, 094502 (2011).
- [27] R. Puebla, O. Abah, and M. Paternostro, *Measurement-based cooling of a nonlinear mechanical resonator*, *Phys. Rev. B* **101**, 245410 (2020).
- [28] J.-s. Yan and J. Jing, *External-level assisted cooling by measurement*, *Phys. Rev. A* **104**, 063105 (2021).
- [29] Z.-y. Jin, J.-s. Yan, and J. Jing, *Measurement-induced nuclear spin polarization*, *Phys. Rev. A* **106**, 062605 (2022).
- [30] M. França Santos, E. Solano, and R. L. de Matos Filho, *Conditional large fock state preparation and field state reconstruction in cavity qed*, *Phys. Rev. Lett.* **87**, 093601 (2001).
- [31] W. Wang, L. Hu, Y. Xu, K. Liu, Y. Ma, S.-B. Zheng, R. Vijay, Y. P. Song, L.-M. Duan, and L. Sun, *Converting quasiclassical states into arbitrary fock state superpositions in a superconducting circuit*, *Phys. Rev. Lett.* **118**, 223604 (2017).
- [32] J. Guerlin, C. Bernu, S. Deléglise, C. Sayrin, S. Gleyzes, S. Kuhr, M. Brune, J.-M. Raimond, and S. Haroche, *Progressive field-state collapse and quantum non-demolition photon counting*, *Nature (London)* **448**, 889 (2007).
- [33] I. Dotsenko, M. Mirrahimi, M. Brune, S. Haroche, J.-M. Raimond, and P. Rouchon, *Quantum feedback by discrete quantum nondemolition measurements: Towards on-demand generation of photon-number states*, *Phys. Rev. A* **80**, 013805 (2009).
- [34] C. Sayrin, I. Dotsenko, X. Zhou, B. Peaudecerf, T. Rybarczyk, S. Gleyzes, P. Rouchon, M. Mirrahimi, H. Amini, M. Brune, J.-M. Raimond, and S. Haroche, *Real-time quantum feedback prepares and stabilizes photon number states*, *Nature (London)* **447**, 73 (2011).
- [35] A. Perret and Y. Bérubé-Lauzière, *Preparation of cavity-fock-state superpositions by reinforcement learning exploiting measurement backaction*, *Phys. Rev. A* **109**, 022609 (2024).
- [36] G. Harel and G. Kurizki, *Fock-state preparation from thermal cavity fields by measurements on resonant atoms*, *Phys. Rev. A* **54**, 5410 (1996).
- [37] A. Delakouras, D. Rodríguez, and J. Cerrillo, *Production of fock mixtures in trapped ions for motional metrology*, *Quantum Sci. Technol.* **9**, 015006 (2023).
- [38] K. Weiher, E. Agudelo, and M. Bohmann, *Conditional nonclassical field generation in cavity qed*, *Phys. Rev. A* **100**, 043812 (2019).